

Intrinsic Spin and Orbital Hall Effects from Orbital Texture

Dongwook Go,¹ Daegeun Jo,¹ Changyoung Kim,^{2,3} and Hyun-Woo Lee^{1,*}

¹*Department of Physics, Pohang University of Science and Technology, Pohang 37673, Korea*

²*Department of Physics and Astronomy, Seoul National University, Seoul 08826, Korea*

³*Center for Correlated Electron Systems, Institute for Basic Science, Seoul 08826, Korea*

 (Received 2 April 2018; revised manuscript received 11 July 2018; published 24 August 2018)

We show theoretically that both the intrinsic spin Hall effect (SHE) and orbital Hall effect (OHE) can arise in centrosymmetric systems through momentum-space orbital texture, which is ubiquitous even in centrosymmetric systems unlike spin texture. The OHE occurs even without spin-orbit coupling (SOC) and is converted into the SHE through SOC. The resulting spin Hall conductivity is large (comparable to that of Pt) but depends on the SOC strength in a nonmonotonic way. This mechanism is stable against orbital quenching. This work suggests a path for an ongoing search for materials with stronger SHE. It also calls for experimental efforts to probe orbital degrees of freedom in the OHE and SHE. Possible ways for experimental detection are briefly discussed.

DOI: [10.1103/PhysRevLett.121.086602](https://doi.org/10.1103/PhysRevLett.121.086602)

The spin Hall effect (SHE) [1–6] is a phenomenon in which an external electric field \mathbf{E} generates a spin current in a transverse direction. When the spin current is injected to a neighboring ferromagnetic layer, it can even switch its magnetization direction [7,8]. The SHE is now regarded as an indispensable tool in spintronics to generate and detect a spin current [5,6]. Of particular interest are intrinsic mechanisms [9–13], which do not rely on impurity scattering. The large SHE in $5d$ transition metals such as Pt is believed to be intrinsic [12–18].

Spin-orbit coupling (SOC) is a crucial element for the intrinsic SHE and has a sizable value only near atomic nuclei [19], where it can be approximated as

$$H_{\text{so}} = \frac{2\alpha_{\text{so}}}{\hbar^2} \mathbf{S} \cdot \mathbf{L}. \quad (1)$$

Here, \mathbf{L} denotes the orbital angular momentum near nuclei. Since the spin \mathbf{S} couples to other degrees of freedom (d.o.f.) only through Eq. (1) in nonmagnets, \mathbf{L} is expected to play important roles for SHE. Although an orbital d.o.f. is taken into account in equilibrium band structure calculations, *dynamical* roles of \mathbf{L} are commonly ignored in the literature. Only for a limited class of systems, it was argued [12,13,20,21] that an Aharonov-Bohm phase generated by orbitals is responsible for SHE and that SHE is closely related to the orbital Hall effect (OHE). Here, OHE refers to an \mathbf{E} -induced transverse flow of \mathbf{L} [22]. Even for these materials, however, there is no experiment that probes roles of \mathbf{L} as far as we are aware. It is partly due to the expectation that \mathbf{L} cannot play any important roles due to orbital quenching [24] in solids.

For centrosymmetric systems with momentum-space orbital texture, we demonstrate that \mathbf{E} generates nonzero \mathbf{L} (even when \mathbf{L} is quenched in equilibrium), which leads

to the intrinsic SHE and OHE since the generated \mathbf{L} is odd in the crystal momentum \mathbf{k} . This mechanism provides not only an alternative theoretical picture to understand the SHE and OHE in Refs. [12,13,20], but also implies that many other systems may exhibit SHE and OHE since the orbital texture is ubiquitous in multiorbital systems. Specifically we demonstrate two points: (i) even when SOC is absent and \mathbf{L} is completely quenched in equilibrium, the orbital texture generates OHE universally; (ii) when SOC is sizable, OHE is efficiently converted into SHE. Thus, the OHE is more fundamental than the SHE in this mechanism. Interestingly, we find that stronger SOC does not necessarily imply enhanced SHE. This result is relevant for ongoing search for materials with strong SHE.

We begin with an illustration of the point (i) for a p -orbital system. We assume $\alpha_{\text{so}} = 0$ since SOC is not essential for (i). We also assume that all orbital degeneracy is lifted and the expectation value of \mathbf{L} is suppressed to zero for all eigenstates. Nevertheless, the orbital texture can be present; the orbital character may vary with \mathbf{k} and from bands to bands. For concreteness, we assume that for $\mathbf{k} = |\mathbf{k}|(\cos \phi, \sin \phi, 0)$ in the $k_z = 0$ plane, the wave function in the upper (lower) band has radial (tangential) p -orbital character, that is $|u_{\mathbf{k}}^{\text{upper}}\rangle \sim |p_{\phi}\rangle$ ($|u_{\mathbf{k}}^{\text{lower}}\rangle \sim |p_{\phi+\pi/2}\rangle$) [Fig. 1(a)]. Here, $|u_{\mathbf{k}}^{\text{upper(lower)}}\rangle$ is the periodic part of the Bloch wave function of the upper (lower) band and $|p_{\phi}\rangle \equiv \cos \phi |p_x\rangle + \sin \phi |p_y\rangle$. Figure 1(b) shows schematically the wave function character of the eigenstates in the lower band at the Fermi surface. Note that the expectation value $\langle \mathbf{L} \rangle$ vanishes for each of these states. Suppose $\mathbf{E} = E_x \hat{x}$ ($E_x > 0$) is then applied to shift \mathbf{k} to $\mathbf{k} + \delta\mathbf{k} = |\mathbf{k} + \delta\mathbf{k}|(\cos(\phi + \delta\phi), \sin(\phi + \delta\phi), 0)$, where $\delta\phi$ is positive (negative) for positive (negative) k_x . Under this

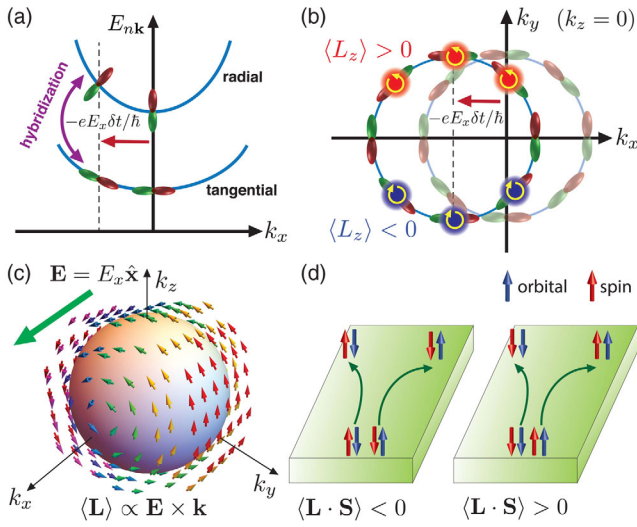


FIG. 1. (a),(b) Illustration of intrinsic OHE from orbital texture in centrosymmetric systems. SOC is ignored for simplicity. (a) Schematic band structure with plots of wave function character at each band. Here, $k_y = k_z = 0$. (b) When an electron in the lower band is pushed from \mathbf{k} to $\mathbf{k} + \delta\mathbf{k}$ by an external electric field $\mathbf{E} \parallel \hat{x}$, positive(negative) $\langle L_z \rangle$ is induced for the non-equilibrium state with $k_y > 0$ ($k_y < 0$). (c) In three-dimensional \mathbf{k} -space, $\langle \mathbf{L} \rangle$ is induced into the direction of $\mathbf{E} \times \mathbf{k}$. This leads to finite $\langle L_z v_y \rangle$, OHE. (d) When SOC is taken into account, SHE occurs in the same or opposite direction of OHE depending on whether the correlation $\langle \mathbf{L} \cdot \mathbf{S} \rangle$ is positive or negative.

\mathbf{k} shift, $|u_{\mathbf{k}+\delta\mathbf{k}}^{\text{lower}}\rangle \sim |p_{\phi+\pi/2}\rangle$, which can be written as $|p_{\phi+\pi/2}\rangle = |p_{\phi+\delta\phi+\pi/2}\rangle + \delta\phi|p_{\phi+\delta\phi}\rangle$, evolves with time to $\exp(-iE_{\mathbf{k}+\delta\mathbf{k}}^{\text{lower}}\delta t/\hbar)|u_{\mathbf{k}+\delta\mathbf{k}}^{\text{lower}}\rangle + \delta\phi\exp(-iE_{\mathbf{k}+\delta\mathbf{k}}^{\text{upper}}\delta t/\hbar)|u_{\mathbf{k}+\delta\mathbf{k}}^{\text{upper}}\rangle$. Thus, an interband superposition is induced by \mathbf{E} . Note that the ratio between the two coefficients of the states $|u_{\mathbf{k}+\delta\mathbf{k}}^{\text{upper/lower}}\rangle$ is *complex*, implying that the superposition contains the component $|p_x\rangle \pm i|p_y\rangle = |L_z = \pm\hbar\rangle$ and its expectation value $\langle L_z \rangle$ is *nonzero*. Thus, even when \mathbf{L} is completely quenched in equilibrium, dynamically induced interband superpositions can have nonzero $\langle \mathbf{L} \rangle$. An explicit calculation results in $\langle \mathbf{L} \rangle \propto \delta\phi\hat{z}$, which points in opposite directions for positive and negative k_y 's [Fig. 1(b)]. This two-dimensional profile of $\langle \mathbf{L} \rangle$ in the $k_z = 0$ plane can be easily extended to a three-dimensional one by rotating Fig. 1(b) around \mathbf{E} . Figure 1(c) shows schematically the resulting three-dimensional profile of $\langle \mathbf{L} \rangle \propto \mathbf{E} \times \mathbf{k}$. Note that although the sum of $\langle \mathbf{L} \rangle$ over occupied superposed states may vanish, the sum of the orbital Hall current $\sim \langle v_y L_z \rangle$ is nonzero. This illustrates an intrinsic mechanism of OHE based on the orbital texture. By the way, the $\langle \mathbf{L} \rangle$ profile in Fig. 1(c) is similar to the *equilibrium* $\langle \mathbf{L} \rangle$ profile in orbital Rashba systems [25,26] despite the crucial difference that $\langle \mathbf{L} \rangle$ in Fig. 1(c) is evaluated for dynamically induced *nonequilibrium* interband superpositions whereas $\langle \mathbf{L} \rangle$ in orbital Rashba systems for *equilibrium* eigenstates.

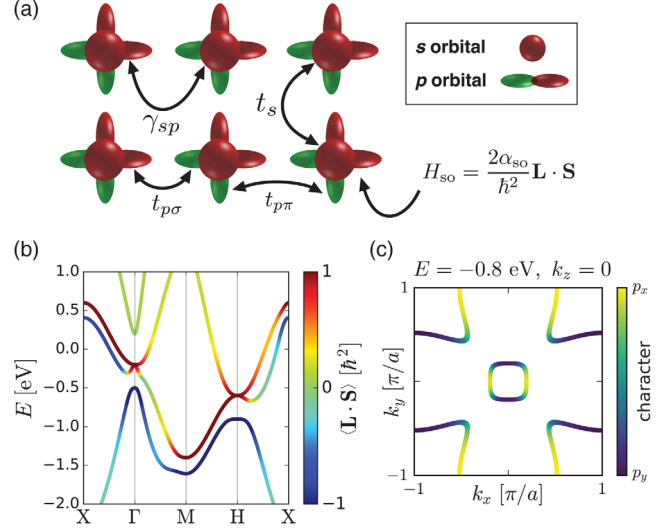


FIG. 2. (a) A tight-binding model on a simple cubic lattice with s , p_x , p_y , and p_z orbitals at each site. The nearest-neighbor hopping amplitude between s orbitals is t_s , and that between p orbitals via $\sigma(\pi)$ bonding is $t_{p\sigma(\pi)}$. An interorbital hopping amplitude from p_x , p_y , or p_z orbital to s orbital is γ_{sp} . (b) Band structure obtained from the tight-binding model. The color represents the correlation $\langle \mathbf{L} \cdot \mathbf{S} \rangle$ for each eigenstate. (c) Wave function character of the eigenstates at $E = -0.8$ eV with $k_z = 0$.

Next we restore SOC. Then, due to the correlation between \mathbf{L} and \mathbf{S} , nonzero $\langle \mathbf{L} \rangle$ in Fig. 1(c) implies $\langle \mathbf{S} \rangle$ to be nonzero. Thus SOC generates SHE as a *concomitant* effect of OHE. The sign of the spin Hall conductivity (SHC) is the same or opposite to that of the orbital Hall conductivity (OHC) depending on whether the correlation is positive or negative (that is, \mathbf{S} is parallel or antiparallel to \mathbf{L}) [Fig. 1(d)].

The orbital texture assumed in Fig. 1(a) occurs even in very trivial systems. To demonstrate this point, we adopt a tight-binding model description of a simple cubic lattice with four orbitals s , p_x , p_y , p_z at each lattice point. Possible nearest-neighbor hoppings are shown in Fig. 2(a) with their hopping amplitudes (see Ref. [27] for details). Figure 2(b) shows the band structure of this system. The three doubly degenerate lower bands have p character whereas the topmost doubly degenerate band (with Γ point band edge at 0.3 eV) has s character. Figure 2(c) shows the orbital character of the states at $E = -0.8$ eV in the $k_z = 0$ plane. Note that the inner (outer) band has radial (tangential) character orbital texture as assumed in Fig. 1(a). We emphasize that the orbital texture arises from the sp hopping γ_{sp} , which mediates the \mathbf{k} -dependent hybridization between p_x , p_y , and p_z orbitals in eigenstates. When $\gamma_{sp} = 0$, the orbital texture disappears. Thus γ_{sp} may be regarded as a measure of the orbital texture strength. Numerical values of the Hamiltonian parameters are (unless mentioned otherwise) as follows; $E_s = 3.2$, $E_{p_x} = E_{p_y} = E_{p_z} = -0.5$ for on-site energies, $t_s = 0.5$, $t_{p\sigma} = 0.5$, $t_{p\pi} = 0.2$, $\gamma_{sp} = 0.5$

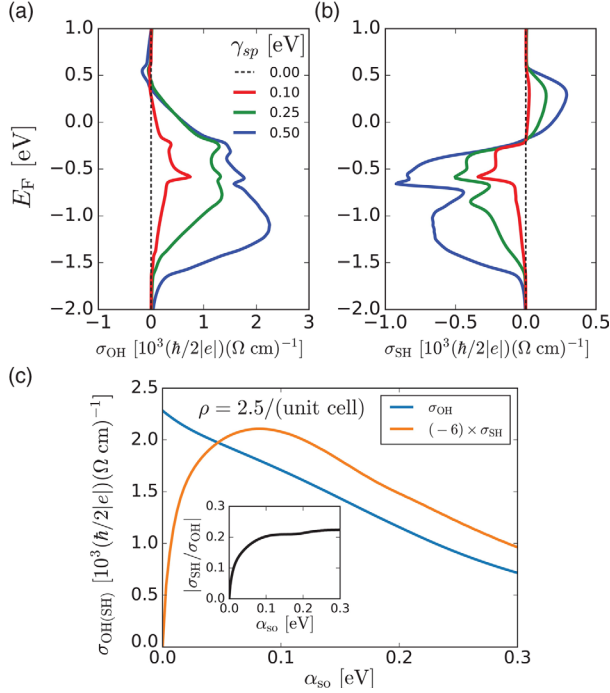


FIG. 3. The E_F dependences of (a) OHC σ_{OH} and (b) SHC σ_{SH} for different values of the sp hopping amplitude γ_{sp} . (c) The SOC dependences of σ_{OH} and σ_{SH} for a fixed electron density, $\rho = 2.5$ /(unit cell). Inset: Conversion efficiency $\sigma_{\text{SH}}/\sigma_{\text{OH}}$ as a function of α_{so} .

for nearest-neighbor hopping amplitudes, and $\alpha_{\text{so}} = 0.1$ for SOC, all in unit of eV.

To assess the role of the orbital texture for the OHE and SHE rigorously, one should go beyond the crude evaluation of the interband superposition given above, which captures only the *initial* evolution of an eigenstate toward its nonequilibrium steady state. For this, we use the Kubo formula,

$$\sigma_{\text{OH(SH)}} = \frac{e}{\hbar} \sum_{n \neq m} \int \frac{d^3 k}{(2\pi)^3} (f_{m\mathbf{k}} - f_{n\mathbf{k}}) \Omega_{nm\mathbf{k}}^{X_z}, \quad (2a)$$

$$\Omega_{nm\mathbf{k}}^{X_z} = \hbar^2 \text{Im} \left(\frac{\langle u_{n\mathbf{k}} | j_y^{X_z} | u_{m\mathbf{k}} \rangle \langle u_{m\mathbf{k}} | v_x | u_{n\mathbf{k}} \rangle}{(E_{n\mathbf{k}} - E_{m\mathbf{k}} + i\eta)^2} \right), \quad (2b)$$

to calculate the OHC (σ_{OH}) and SHC (σ_{SH}) for the tight-binding model with the orbital texture. Here $j_y^{X_z} = (v_y X_z + X_z v_y)/2$ is the conventional orbital (spin) current operator with $X_z = L_z (S_z)$, $v_{x(y)}$ is the velocity operator along the $x(y)$ direction, and $f_{n\mathbf{k}}$ is the Fermi-Dirac distribution function. In view of the illustration in Fig. 1, $\Omega_{nm\mathbf{k}}^{X_z}$ amounts to the contribution to $\sigma_{\text{OH(SH)}}$ from the interband superposition between the bands n and m . Figures 3(a) and 3(b) show, respectively, the calculated σ_{OH} and σ_{SH} as a function of the Fermi energy E_F for different orbital texture strengths. Note that both σ_{OH} and σ_{SH} vanish for $\gamma_{sp} = 0$ and grow with increasing

γ_{sp} . Thus the orbital texture is crucial not only for OHE but also for SHE. Note that for $\gamma_{sp} \gtrsim 0.1$ eV, both σ_{OH} and σ_{SH} can be gigantic $\sim 10^3 \hbar/2|e|$ ($\Omega \text{ cm})^{-1}$, which is comparable to SHC of Pt [14,17,28].

Figure 3(c) shows the SOC strength (α_{so}) dependence of σ_{OH} and σ_{SH} (see Ref. [27] for further details) for a fixed electron density $\rho = 2.5$ electrons per unit cell, which corresponds to $E_F \approx -0.7$ eV though precise E_F value varies with α_{so} . Note that σ_{OH} is nonzero even when $\alpha_{\text{so}} = 0$, confirming that OHE can arise even without SOC. On the other hand, $\sigma_{\text{SH}} = 0$ for $\alpha_{\text{so}} = 0$ and increases as α_{so} is turned on. These results are consistent with the interpretation that OHE arises first and SHE is converted from OHE through SOC. An additional support to this interpretation comes from microscopic (\mathbf{k} - and band-resolved) contributions to σ_{OH} and σ_{SH} [27], which qualitatively match with each other once the correlation $\langle \mathbf{L} \cdot \mathbf{S} \rangle$ distribution in Fig. 2(b) is taken into account. Interestingly, σ_{SH} decreases when α_{so} goes beyond a threshold value (~ 0.1 eV). Such nonmonotonic dependence on α_{so} can be understood as a combined effect of two trends: enhanced SOC may reduce σ_{OH} [Fig. 3(c)] and the conversion efficiency from OHE to SHE, $\sigma_{\text{SH}}/\sigma_{\text{OH}}$ [inset in Fig. 3(c)], saturates once a system enters the strong SOC regime. This result implies that materials with overly strong SOC may not be good choices for large SHC.

Interestingly, OHC and SHC remain stable against crystal field splitting. When the on-site energies of p_x and p_y orbitals are shifted by $\pm \Delta_{\text{cf}}$, respectively, we find [27] that $\sigma_{\text{OH(SH)}}$ remains intact even for Δ_{cf} as large as 0.3 eV because orbital degeneracy between p -character bands is already lifted by γ_{sp} for most \mathbf{k} points except a few high symmetry points, such as Γ and H [Fig. 2(b)].

Next we compare our work with other theoretical works. For two-dimensional Rashba systems, Ref. [10] reports that momentum-space spin texture generates an interband superposition upon the application of $\mathbf{E} = E_x \hat{x}$ and $\langle S_z \rangle$ for the superposition has opposite signs for opposite signs of k_y 's. This mechanism (Fig. 1 of Ref. [10]) is thus very similar to ours (Fig. 1 of this Letter) and our work may be regarded as an orbital counterpart of Ref. [10]. There are clear differences, however. Reference [10] completely ignores the orbital d.o.f. and is applicable only to non-centrosymmetric systems, whereas ours is applicable to centrosymmetric systems. The result in Ref. [10] is significantly affected by the vertex correction [34], which captures effects of impurity scattering, whereas our result is not since the vertex corrections for σ_{SH} and σ_{OH} vanish in the weak scattering limit due to the inversion symmetry [12,35,36].

For $4d$ and $5d$ transition metals, Refs. [12,13] report the interatomic hopping between s and d orbitals to be important for the OHE and SHE and interpret the result in terms of the Aharonov-Bohm phase. We argue that the result may be interpreted alternatively as a d -orbital version

of the orbital-texture-based mechanism (Fig. 1). In centrosymmetric transition metals of fcc or bcc crystal structure, the sd hopping between nearest neighbor atoms generates orbital texture in d -character bands. Then for $\mathbf{E} = E_x \hat{\mathbf{x}}$, the resulting interband superpositions between d -character bands contain components such as $|d_{xz}\rangle \pm i|d_{yz}\rangle = |L_z = \pm \hbar\rangle$ and $|d_{x^2-y^2}\rangle \pm i|d_{xy}\rangle = |L_z = \pm 2\hbar\rangle$, resulting in OHE and SHE. See the Discussion section for the example of fcc Pt.

For three-dimensional semiconductors such as GaAs [9] and HgTe [37], roles of the momentum-space Berry curvature on the SHE are analyzed near the Γ point, at which p -character bands become fourfold degenerate. Since the analyses ignore the inversion symmetry breaking in the semiconductors, they apply to our model system [Fig. 2(a)] as well and explain small narrow peaks (on top of large broad background) at $E_F \approx -0.2$ and -0.7 eV in Fig. 3(b), which arise from the fourfold degenerate Γ and H points [Fig. 2(b)]. Although roles of \mathbf{L} are not evident in the analyses, they may also be interpreted by the orbital-texture-based mechanism except that the origin of the orbital texture is different; in the zinc blende structure of GaAs and HgTe, nearest neighbor hoppings between the p_x , p_y , and p_z orbitals *themselves* can generate orbital texture in p -character valence bands. This interpretation explains OHE in hole-doped Si [35] naturally, which may be regarded as the vanishing SOC limit of hole-doped GaAs. It also predicts p -character bands with the total spin $J = 1/2$ and $3/2$ to contribute to SHC oppositely due to their opposite correlation $\mathbf{L} \cdot \mathbf{S}$, which is consistent with the first-principles calculation results [18,38], when both types of bands are partially occupied in hole-doped GaAs.

The SHE in semiconductors is examined also for s -character conduction bands [18,29] near the Γ point. Related with the result, we remark that the orbital-texture-based mechanism applies even for the s -character band in Fig. 2(b) since the s -character band has partial p character due to the sp hopping and thus can have nonzero $\langle \mathbf{L} \rangle$ through the interband superpositions with p -character bands. To demonstrate this point, we calculate $\Omega_{nm\mathbf{k}}^{L_z}$ [Eq. (2b)] near $\mathbf{k} = \mathbf{0}$ with m denoting the s -character band and n one of the p -character bands in the limit $\alpha_{\text{so}} = 0$ [39] and $\Delta_{\text{cf}} = 0$. Considering that $-\Omega_{nm\mathbf{k}}^{L_z}$ may alternatively be interpreted [Eq. (2a)] as a contribution to the OHE in p -character bands through their interband superposition with the s -character band, $\Omega_{nm\mathbf{k}}^{L_z}$ may be evaluated from properties of p -character bands. For the p -character bands, we obtain [27] the Berry curvature $\Omega^{(p)}(\mathbf{k})$ arising from their interband superposition with the s -character band,

$$\Omega^{(p)}(\mathbf{k}) = -2\lambda_{sp}\mathbf{L}^{(p)} + \mathcal{O}(\mathbf{k})^2, \quad (3)$$

where $\lambda_{sp} = a^2\gamma_{sp}^2/2\hbar E_g^2$, a is the lattice spacing of the cubic lattice in Fig. 2(a), E_g is the band gap between the

s - and p -character bands, and $\mathbf{L}^{(p)}$ is the operator \mathbf{L} projected to the p -character sub-Hilbert space. When the space is represented by the three basis orbitals $|p_x\rangle$, $|p_y\rangle$, $|p_z\rangle$, $\mathbf{L}^{(p)} = (L_x^{(p)}, L_y^{(p)}, L_z^{(p)})$ is represented by the following elements:

$$(L_\alpha^{(p)})_{\beta\gamma} = -i\hbar\epsilon_{\alpha\beta\gamma}. \quad (4)$$

The matrices satisfy the usual angular momentum commutation relations. $\Omega^{(p)}(\mathbf{k})$ is thus non-Abelian [9]. The non-Abelian nature of $\Omega^{(p)}(\mathbf{k})$ is a consequence of symmetries since Abelian Berry curvatures are forced to vanish [40] by the combination of the space inversion and the time-reversal symmetries. Only non-Abelian Berry curvatures can survive the symmetry constraints. When real wave functions are used as bases of representations as in Eq. (4), the symmetries force only diagonal components of the \mathbf{k} -space Berry curvature to vanish and off-diagonal components are free from such constraints. It is these off-diagonal components of $\Omega^{(p)}(\mathbf{k})$ that generate intrinsic OHE. From $\Omega^{(p)}(\mathbf{k})$, one obtains [27] near $\mathbf{k} = \mathbf{0}$,

$$\Omega_{nm\mathbf{k}}^{L_z} \approx \frac{1}{4} \sum_{\mu,\nu=x,y,z} \text{Re}[\langle u_{n\mathbf{k}} | p_\mu \rangle (L_z^{(p)} \Omega_z^{(p)})_{\mu\nu} \langle p_\nu | u_{n\mathbf{k}} \rangle], \quad (5)$$

which confirms OHE in the s -character band through its interband superposition with the p -character bands.

Discussion.—In addition to the sp hybridized system in a simple cubic lattice [Fig. 2(a)], we perform calculations for other orbital hybridizations in other centrosymmetric systems and obtain similar results [41]. For fcc Pt, in particular, we verify [27] that as the strength of the orbital texture is gradually reduced in calculation, its SHC reduces to zero just like Fig. 3(b). This indicates that the orbital-texture-based mechanism is the dominant mechanism of SHE in fcc Pt and that strong SOC alone is not sufficient and orbital texture is crucial.

Since orbital (spin) currents are not directly measurable, the OHE (SHE) should be probed through orbital (spin) moments accumulated at the edges of the systems [42]. The magneto-optical Kerr effect is used in Refs. [43,44] to probe accumulated magnetic moments at the edges. To differentiate the orbital and spin accumulations, one may utilize x-ray magnetic circular dichroism [45,46] or electron energy-loss magnetic circular dichroism [47,48].

Since the orbital (spin) is not conserved, the connection between edge accumulation and $\sigma_{\text{OH(SH)}}$ is not straightforward and there is ongoing discussion [49]. To assess this connection, we calculate the nonequilibrium orbital (spin) density generated by \mathbf{E} as a function of position for a finite size system. We verify [27] that two opposite edges have opposite signs of orbital (spin) accumulations and for a given edge, the orbital (spin) accumulations at two different E_F values (-1.3 and $+0.0$ eV, respectively) have the opposite(same) signs, which agree qualitatively with the

behaviors of $\sigma_{\text{OH(SH)}}$ in Fig. 3. However, further study is needed to clarify the connection, which goes beyond the scope of this Letter.

To conclude, we demonstrated that orbital texture in multiorbital centrosymmetric systems can generate OHE, which is then converted to SHE by SOC. We found that SHE does not necessarily monotonically increase with SOC strength, which provides one possible explanation why experiments (see Table III in Refs. [50,51]) on f orbital rare-earth systems with very strong SOC find σ_{SH} to be only $100 \sim 200(\hbar/2|e|)$ ($\Omega \text{ cm}$)⁻¹, which is about 1 order of magnitude smaller than that for Pt. According to our preliminary calculation [41], systems with much weaker SOC such as vanadium can have $\sigma_{\text{SH}} \sim -200(\hbar/2|e|)$ ($\Omega \text{ cm}$)⁻¹, which is converted from exceptionally large $\sigma_{\text{OH}} \sim 10^4(\hbar/2|e|)$ ($\Omega \text{ cm}$)⁻¹ by weak SOC. Considering the importance of orbital hybridization, we argue that stronger OHE and SHE may be realized in binary compounds, in which orbitals of different character from different atomic elements share similar energies and generate strong orbital hybridization. Our result calls for experimental efforts to probe dynamically generated \mathbf{L} in materials with strong OHE or SHE.

D. G. acknowledges fruitful discussion with Wonsung Jung and Yuriy Mokrousov. We thank E. I. Rashba for valuable comments on the similarity between Eq. (3) and Ref. [29]. D. G. was supported by the Global Ph.D. Fellowship Program by the National Research Foundation of Korea (Grant No. 2014H1A2A1019219). D. G., D. J., and H.-W. L. were supported by the Samsung Science & Technology Foundation (Grant No. BA-1501-07). Work on the Berry curvature by C. K. was supported by the research program of Institute for Basic Science (Grant No. IBS-R009-G2).

*hwl@postech.ac.kr

- [1] M. I. D'yakonov and V. I. Perel, *JETP Lett.* **13**, 467 (1971).
- [2] J. E. Hirsch, *Phys. Rev. Lett.* **83**, 1834 (1999).
- [3] H.-A. Engel, E. I. Rashba, and B. I. Halperin, in *Handbook of Magnetism and Advanced Magnetic Materials*, edited by H. Kronmüller and S. Parkin (Wiley, Chichester, 2006), Vol. 5, p. 2858.
- [4] J. Schliemann, *Int. J. Mod. Phys. B* **20**, 1015 (2006).
- [5] Y. Niimi and Y. Otani, *Rep. Prog. Phys.* **78**, 124501 (2015).
- [6] J. Sinova, S. O. Valenzuela, J. Wunderlich, C. H. Back, and T. Jungwirth, *Rev. Mod. Phys.* **87**, 1213 (2015).
- [7] L. Liu, O. J. Lee, T. J. Gudmundsen, D. C. Ralph, and R. A. Buhrman, *Phys. Rev. Lett.* **109**, 096602 (2012).
- [8] L. Liu, C.-F. Pai, Y. Li, H. W. Tseng, D. C. Ralph, and R. A. Buhrman, *Science* **336**, 555 (2012).
- [9] S. Murakami, N. Nagaosa, and S.-C. Zhang, *Science* **301**, 1348 (2003).
- [10] J. Sinova, D. Culcer, Q. Niu, N. A. Sinitsyn, T. Jungwirth, and A. H. MacDonald, *Phys. Rev. Lett.* **92**, 126603 (2004).
- [11] S.-Q. Shen, *Phys. Rev. B* **70**, 081311 (2004).
- [12] T. Tanaka, H. Kontani, M. Naito, T. Naito, D. S. Hirashima, K. Yamada, and J. Inoue, *Phys. Rev. B* **77**, 165117 (2008).
- [13] H. Kontani, T. Tanaka, D. S. Hirashima, K. Yamada, and J. Inoue, *Phys. Rev. Lett.* **102**, 016601 (2009).
- [14] G. Y. Guo, S. Murakami, T.-W. Chen, and N. Nagaosa, *Phys. Rev. Lett.* **100**, 096401 (2008).
- [15] F. Freimuth, S. Blügel, and Y. Mokrousov, *Phys. Rev. Lett.* **105**, 246602 (2010).
- [16] M. Morota, Y. Niimi, K. Ohnishi, D. H. Wei, T. Tanaka, H. Kontani, T. Kimura, and Y. Otani, *Phys. Rev. B* **83**, 174405 (2011).
- [17] E. Sagasta, Y. Omori, M. Isasa, M. Gradhand, L. E. Hueso, Y. Niimi, Y. C. Otani, and F. Casanova, *Phys. Rev. B* **94**, 060412 (2016).
- [18] Y. Yao and Z. Fang, *Phys. Rev. Lett.* **95**, 156601 (2005).
- [19] G. Bihlmayer, Y. M. Koroteev, P. M. Echenique, E. V. Chulkov, and S. Blügel, *Surf. Sci.* **600**, 3888 (2006).
- [20] H. Kontani, T. Tanaka, D. S. Hirashima, K. Yamada, and J. Inoue, *Phys. Rev. Lett.* **100**, 096601 (2008).
- [21] T. Tanaka and H. Kontani, *Phys. Rev. B* **81**, 224401 (2010).
- [22] We emphasize that \mathbf{L} denotes the orbital angular momentum near atomic nuclei, which differs from \mathbf{L} in Refs. [23,38].
- [23] S. Zhang and Z. Yang, *Phys. Rev. Lett.* **94**, 066602 (2005).
- [24] C. Kittel, *Introduction to Solid State Physics* (Wiley, New York, 2004).
- [25] S. R. Park, C. H. Kim, J. Yu, J. H. Han, and C. Kim, *Phys. Rev. Lett.* **107**, 156803 (2011).
- [26] S. R. Park and C. Kim, *J. Electron Spectrosc. Relat. Phenom.* **201**, 6 (2015).
- [27] See Supplemental Material at <http://link.aps.org/supplemental/10.1103/PhysRevLett.121.086602> for details of methods and results, which includes Refs. [9,12,14,17, 28–33].
- [28] T. Kimura, Y. Otani, T. Sato, S. Takahashi, and S. Maekawa, *Phys. Rev. Lett.* **98**, 156601 (2007).
- [29] E. I. Rashba, *Semiconductors* **42**, 905 (2008).
- [30] P. Nozières and C. Lewiner, *J. Phys. (Paris)* **34**, 901 (1973).
- [31] R. Winkler, *Spin-Orbit Coupling Effects in Two-Dimensional Electron and Hole Systems*, Springer Tracts in Modern Physics (Springer, Verlag, Berlin, Heidelberg, 2003).
- [32] M.-C. Chang and Q. Niu, *J. Phys. Condens. Matter* **20**, 193202 (2008).
- [33] D. A. Papaconstantopoulos, *Handbook of the Band Structure of Elemental Solids* (Springer, New York, 2015).
- [34] J. I. Inoue, G. E. W. Bauer, and L. W. Molenkamp, *Phys. Rev. B* **70**, 041303 (2004).
- [35] B. A. Bernevig, T. L. Hughes, and S.-C. Zhang, *Phys. Rev. Lett.* **95**, 066601 (2005).
- [36] S. Murakami, *Phys. Rev. B* **69**, 241202 (2004).
- [37] S. Murakami, N. Nagaosa, and S.-C. Zhang, *Phys. Rev. Lett.* **93**, 156804 (2004).
- [38] G. Y. Guo, Y. Yao, and Q. Niu, *Phys. Rev. Lett.* **94**, 226601 (2005).
- [39] A similar result can be derived for the opposite limit. When α_{so} is very large, p -character bands split into the total angular momentum $j = 3/2$ multiplet and $j = 1/2$ multiplet. For each multiplet, the non-Abelian Berry curvature [27] does not diverge at the Γ point and is collinear to $\mathbf{J} = \mathbf{L} + \mathbf{S}$. For this limit of strong SOC, similar Berry curvature expressions are obtained for the Kane model [29–32].

- [40] M. Gradhand, D. V. Fedorov, F. Pientka, P. Zahn, I. Mertig, and B. L. Gyrfy, *J. Phys. Condens. Matter* **24**, 213202 (2012).
- [41] D. Jo, D. Go, and H.-W. Lee, [arXiv:1808.05546](https://arxiv.org/abs/1808.05546).
- [42] J. Sinova, S. Murakami, S.-Q. Shen, and M.-S. Choi, *Solid State Commun.* **138**, 214 (2006).
- [43] Y. K. Kato, R. C. Myers, A. C. Gossard, and D. D. Awschalom, *Science* **306**, 1910 (2004).
- [44] C. Stamm, C. Murer, M. Berritta, J. Feng, M. Gabureac, P. M. Oppeneer, and P. Gambardella, *Phys. Rev. Lett.* **119**, 087203 (2017).
- [45] W. L. O'Brien and B. P. Tonner, *Phys. Rev. B* **50**, 12672 (1994).
- [46] S. Bonetti, *J. Phys. Condens. Matter* **29**, 133004 (2017).
- [47] P. Schattschneider, S. Rubino, C. Hebert, J. Ruzs, J. Kunes, J. Novak, P. Novak, E. Carilino, M. Fabrizio, G. Panaccione, and G. Rossi, *Nature (London)* **441**, 486 (2006).
- [48] J. Verbeeck, H. Tian, and P. Schattschneider, *Nature (London)* **467**, 301 (2010).
- [49] J. Shi, P. Zhang, D. Xiao, and Q. Niu, *Phys. Rev. Lett.* **96**, 076604 (2006).
- [50] N. Reynolds, P. Jadaun, J. T. Heron, C. L. Jermain, J. Gibbons, R. Collette, R. A. Buhrman, D. G. Schlom, and D. C. Ralph, *Phys. Rev. B* **95**, 064412 (2017).
- [51] K. Ueda, C.-F. Pai, A. J. Tan, M. Mann, and G. S. D. Beach, *Appl. Phys. Lett.* **108**, 232405 (2016).